

# On the virialization threshold for halo mass functions

Ronaldo C. Batista<sup>a</sup>

<sup>a</sup>Escola de Ciências e Tecnologia, Universidade Federal do Rio Grande do Norte, Campus Universitário Lagoa Nova, 59078-970, Natal, RN, Brazil.

E-mail: [rbatista@ect.ufrn.br](mailto:rbatista@ect.ufrn.br)

**Abstract.** In a recent study by Euclid collaboration, the halo mass function (HMF) has been fitted with accuracy better than 1% for the  $\Lambda$ CDM model. Several parameters were introduced and fitted against N-body simulations, assuming the usual linearly extrapolated matter density contrast at the collapse time,  $\delta_c$ , as a basic threshold for halo formation. As a result, a new function that multiplies  $\delta_c$  was introduced, producing an effective threshold that varies both with redshift and mass scale. We show that the redshift evolution of this effective threshold is similar to the one of the linear extrapolated matter density contrast at the virialization time,  $\delta_v$ . Assuming the Euclid HMF as a fiducial model, we refit the Sheth-Tormen (ST) HMF using  $\delta_v$  as a threshold. This new fit improves the agreement between ST-HMF and the Euclid one with respect to Despali et al. (2016) fit, specially at high masses. Interestingly, the parameters  $a$  and  $p$  in this refit have values closer to the Press-Schechter limit of the ST-HMF, showing that the use of  $\delta_v$  can provide semi-analytical HMF less dependent on extra parameters. Moreover, we analyze the consistency of the ST-HMF fitted with  $\delta_v$  in smooth dark energy models with time-varying equation of state, finding an overall good agreement with the evolution of halo abundances expected from the linear evolution of perturbations and the Euclid HMF extrapolated to these scenarios. These findings suggest that the use  $\delta_v$  as a basic function to describe the threshold for halo formation can be a good guide when considering extrapolations for models beyond  $\Lambda$ CDM, which are typically harder to study in simulations. We also provide a fitting formula for  $\delta_v$  in the  $\Lambda$ CDM model and a code to compute it for smooth dark energy described by the  $w_0w_a$  parametrization.

---

## Contents

<b>1</b>	<b>Introduction</b>	<b>1</b>
<b>2</b>	<b>Thresholds definitions</b>	<b>3</b>
<b>3</b>	<b>The effective threshold in the E-HMF and <math>\delta_v</math></b>	<b>4</b>
<b>4</b>	<b>Sheth-Tormen halo mass function with <math>\delta_v</math></b>	<b>6</b>
<b>5</b>	<b>Beyond <math>\Lambda</math>CDM models</b>	<b>8</b>
5.1	Constant EoS	10
5.2	Time varying EoS	10
<b>6</b>	<b>Conclusions</b>	<b>13</b>
<b>A</b>	<b><math>\delta_v</math> fit for <math>\Lambda</math>CDM and a general code for its computation</b>	<b>14</b>

---

## 1 Introduction

Since the first analytical proposal of a Halo Mass Function (HMF) by Press and Schechter (PS) [1], several semi-analytical and numerical studies on the topic have proposed alternative formulations, e.g., [2–8]. See [9] for an overview of several of these proposals. One of the key ingredients in the PS formulation, and in many others based in the Sheth-Tormen (ST) template [2], is the value of the critical density for the formation of halos,  $\delta_c$ , which mainly controls the exponential decay of the number of massive halos. Ideally, this parameter represents the value of the extrapolated linearly evolved matter contrast,  $\delta_m$ , above which halos are formed. For many years following the PS proposal, several distinct values for this threshold were used, e.g., [10–12]. Following the suggestions in [13, 14], the use of  $\delta_c \simeq 1.686$ , the value calculated for Einstein-de-Sitter (EdS) cosmology using the framework of the Spherical Collapse (SC) model [15, 16] at the moment of collapse, became standard.

In [17], a reparametrization of this value was introduced, such that  $\delta_c^2 \rightarrow a\delta_c^2$ , where  $a = 0.707$ . The value of  $a$  can vary when fitted against distinct N-body simulations, for a compilation of values see [18], but  $a < 1$  is obtained in almost all cases. This indicates that the usual threshold for halo formation must be reduced to describe better the halo abundances seen in numerical simulations. In  $\Lambda$ CDM cosmology,  $\delta_c$  is no longer constant. It is well known that  $\delta_c$  has a slight decay when  $\Lambda$  becomes important for the background evolution [19–21]. Given this small variation, assuming the constant EdS value of  $\delta_c$  became usual.

Recently, it was shown by the Euclid collaboration that better than 1% accurate HMF can be obtained in the  $\Lambda$ CDM model at the cost of including new mass and redshift-dependent functions, [8] (we refer to this formulation as E-HMF). In particular, the effective threshold in the E-HMF is given by  $a_R\Omega_m^{a_z}\delta_c^2$ , where  $a_R$  depends on the mass scale and  $\Omega_m^{a_z}\delta_c^2$  is redshift-dependent. The value of  $a_z$  was shown to depend on the halo-finding algorithm and ranging between  $-0.0693 \leq a_z \leq -0.0523$ . Therefore, as  $\Lambda$  begins to dominate the background expansion and  $\Omega_m$  decays, the effective threshold increases at low- $z$ . Thus, one can understand that the slight decay of  $\delta_c$  does not correctly represent the effects of  $\Lambda$  on the HMF threshold

and the function  $\Omega_m^{a_z}$  compensates for this decay, introducing an increase in the effective threshold at low- $z$ . This kind of behaviour for the effective threshold was also found in [22], but note that this work aimed to improve the accuracy of the halo model, not the HMF itself.

As suggest in [23–25], one can define another theoretical threshold for halo formation,  $\delta_v$ , associated with virialization time. The definitions for the collapse and virialization threshold are:

$$\delta_c = \delta_m^L(z_c) \quad \text{and} \quad \delta_v = \delta_m^L(z_v), \quad (1.1)$$

where  $\delta_m^L$  is the linearly evolved matter perturbations at the redshift of collapse,  $z_c$ , or virialization,  $z_v$ . Both of these quantities are computed in the framework of the SC model. For EdS, there is an analytical solution giving a constant  $\delta_v \simeq 1.583$ . If one substitutes  $\delta_c$  by  $\delta_v$  in HMFs, the threshold is reduced, as effectively done by the values of  $a$  in the ST formulation, indicating the virialization time can provide a better description of the abundance of halos, especially at the high-mass tail of HMFs.

Moreover, the increase of the effective threshold at low- $z$  naturally occurs for  $\delta_v$  [26–28]. Therefore, besides giving a lower baseline value for the effective threshold,  $\delta_v$  also gives the qualitatively expected redshift variation, as seen in the E-HMF. Given these two desirable features, it is very tempting to consider reparametrizations of HMFs using  $\delta_v$  instead of  $\delta_c$ .

This idea was explored in the context of clustering DE [26], where the following substitution was proposed  $a\delta_c^2 \rightarrow \tilde{a}\delta_v^2$ , where  $\tilde{a} = 0.803$  is chosen such that the EdS limit of the ST-HMF is unchanged. The main advantage of this approach is a more consistent computation of the threshold in the presence of non-matter fluctuations, see [28, 29] for more details. Moreover, as explained in [29], is it not possible to numerically compute  $\delta_c$  in clustering DE models with arbitrary sound speed.

In this work, we will further explore the possibility of using  $\delta_v$  instead of  $\delta_c$  in HMFs, focusing in the  $\Lambda$ CDM model. First, we will show that the redshift-dependent part of the E-HMF is well described by a simple power-law function  $\delta_v$ , with precision better 0.7% for  $0.2 \leq \Omega_m^0 \leq 0.4$ , indicating that the correspondence between the functions is not a coincidence for a particular value of  $\Omega_m^0$ . Then we proceed with a reparametrization of the ST-HMF using  $\delta_v$  and assuming the E-HMF as a fiducial model, showing that this refit agrees better with E-HMF than the HMF fit given by [6]. As a result, we find that the refitted ST parameters  $a$  and  $p$  get closer to the values that reproduce the PS-HMF. We also analyse how the ST-HMF refitted with  $\delta_v$  behaves when considering smooth DE models with  $w \neq -1$ .

The plan of this paper is as follows. In section 2 we review and discuss the collapse and virialization definitions for the thresholds. In section 3, we compare the redshift-dependent part of the E-HMF with  $\delta_v$  and reexpress  $\Omega_m^{a_z}\delta_c^2$  as a function of  $\delta_v$ . In section 4, substituting  $\delta_c$  by  $\delta_v$ , we refit the ST-HMF, assuming the E-HMF as a fiducial model. In section 5, we analyse the consistency of the ST-HMF refitted with  $\delta_v$  for smooth DE models described by the  $w_0w_a$  parametrization. We conclude in section 6 and provide a representation of  $\delta_v$  in terms of a well-known fit for  $\delta_c$  for  $\Lambda$ CDM model in Appendix A, also indicating a repository where a code to compute  $\delta_v$  assuming the  $w_0w_a$  parametrization can be found.

Throughout this paper, we assume as baseline the  $\Lambda$ CDM model with parameters:  $h = 0.7$ ,  $\Omega_c^0 h^2 = 0.125$ ,  $\Omega_b^0 h^2 = 0.022$ ,  $A_s = 2 \times 10^{-9}$ ,  $n_s = 0.965$ ,  $\tau = 0.06$ ,  $m_\nu = 0.06$  and  $\Omega_k^0 = 0$ . In some examples, we vary  $\Omega_m^0$  by changing only  $\Omega_c^0 h^2$ . When analysing DE models described by the  $w_0w_a$  parametrization, all the other parameters are kept fixed at the  $\Lambda$ CDM values. The computation of the matter power spectrum is made with CAMB [30].

## 2 Thresholds definitions

Let us first revise how the collapse and virialization thresholds for the formation of halos are defined and their redshift dependence. For a more detailed discussion and calculation methods, see [28] and references therein. Both quantities are derived in the framework of the SC model, which can be summarised by the equations

$$\ddot{R} = -\frac{GM}{R^2} \quad \text{and} \quad M = \frac{4\pi}{3} R^3 \bar{\rho}_m (1 + \delta_m(t)) = \text{const}, \quad (2.1)$$

where  $R$  is the radius of a spherical shell that encloses the conserved mass  $M$ ,  $\bar{\rho}_m$  is the background matter density and  $\delta_m$  the matter density contrast with no radial variation within the shell.

The usual  $\delta_c$  threshold is given by the linearly extrapolated density contrast at the redshift of collapse,  $z_c$ . The collapse time is associated with the moment at which the radius of the spherical shell goes to zero, or equivalently when the nonlinearly evolved density contrast associated with that shell diverges. Thus we have:

$$\lim_{z \rightarrow z_c^+} \delta_m^{NL}(z) = +\infty \quad \text{and} \quad \delta_c(z_c) = \delta_m^L(z_c), \quad (2.2)$$

where superscripts  $NL$  and  $L$  represent the nonlinear and linear evolutions of  $\delta_m$ , respectively.

The virialization threshold, introduced in [23–25], is given by the linearly extrapolated density contrast at the redshift of virialization,  $z_v$ ,

$$\delta_v(z_v) = \delta_m^L(z_v). \quad (2.3)$$

The moment of virialization is also given by the SC model, when virial equilibrium is achieved. Following [31], the virialization time is determined when the equation below is satisfied

$$\frac{1}{R^2} \left( \frac{dR}{dt} \right)^2 + \frac{1}{R} \frac{d^2 R}{dt^2} = 0 \quad (2.4)$$

In EdS, the moment of virialization is such that we have

$$\delta_v \simeq 1.583 \quad \text{and} \quad \Delta_v = \frac{\rho_m(z_v)}{\bar{\rho}_m(z_v)} \simeq 146.8, \quad (2.5)$$

where  $\rho_m(z) = \bar{\rho}_m(z) [1 + \delta_m^{NL}(z)]$  is the total matter density. Note that  $\Delta_v$  is not the usual virialization overdensity, which is given by  $\Delta = \rho_m(z_v) / \bar{\rho}_m(z_c) \simeq 177.7$ .

It is interesting to note that the virialization equation can be generalised to include other components, such as smooth or clustering DE [26, 27, 31–33], whereas the collapse definition is mostly insensitive to other ingredients that participate in the collapse process. Though in general  $\delta_m^{NL}$  depends on the background evolution and other clustering components, near the collapse time, it is growing nearly exponentially, responding essentially to its own nonlinear value. Thus, the background evolution, and possibly other subdominant fluctuations, have very small impact on the value of  $\delta_c$ , typically less than 1% with respect to the EdS value [28].

Summarising, in the EdS model, the two thresholds can be analytically computed and are constants:

$$\delta_{c\text{EdS}} \simeq 1.686 \quad \text{and} \quad \delta_{v\text{EdS}} \simeq 1.583. \quad (2.6)$$

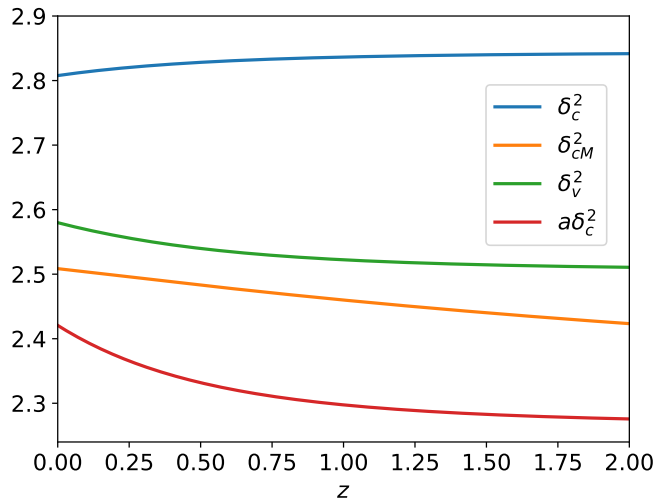


**Figure 1.** Evolution of  $\delta_c^2$ ,  $\delta_{cM}^2$ ,  $\delta_v^2$  and  $a\delta_c^2$  as a function of redshift in the  $\Lambda$ CDM model with  $\Omega_m^0 = 0.3$ ,  $a_z = -0.0658$  and  $a_R = 0.7965$  (corresponding to a mass-scale  $10^{14}M_\odot h^{-1}$ ).

When DE begins to dominate the expansion, they become redshift-dependent. Whereas  $\delta_c$  has a slight decay when DE becomes important,  $\delta_v$  presents a mild growth, see figure 1.

In this context, it is also interesting to mention that the following threshold

$$\delta_{cM} = 1.59 + 0.3114 \times \ln \sigma_8(z), \quad (2.7)$$

proposed in [22] to improve the accuracy of the nonlinear power-spectrum computed via the halo model, also has a smaller value than  $\delta_c$  and a mild growth at low- $z$ . In figure 1 we show the evolution of the squares of  $\delta_c$ ,  $\delta_v$ ,  $\delta_{cM}$  and also the redshift-dependent part of the effective threshold in the E-HMF,  $a\delta_c^2$ , which will discuss in more detail in section 3. Assuming that the best representation of the effective threshold is given by  $a\delta_c^2$ , where  $a$  is given by (3.5), we clearly see that usual  $\delta_c$  is both higher and has the opposite redshift variation. On the other hand,  $\delta_v^2$  is closer to  $a\delta_c^2$  and also increases at low- $z$ . The fit given in (2.7) was obtained in order to improve the accuracy of the halo model, and not necessarily the HMF. But it is also clear that its behaviour is more compatible with  $a\delta_c^2$  than  $\delta_c^2$ .

### 3 The effective threshold in the E-HMF and $\delta_v$

In this section, we analyse how the effective threshold of E-HMF is related to  $\delta_v$  and define the main quantities of interest. The comoving number density of halos per mass interval is given by

$$\frac{dn}{dM} = \frac{\rho_m}{M} \nu f(\nu) \frac{d \ln \nu}{dM}, \quad (3.1)$$

where  $\nu f(\nu)$  is the multiplicity function,  $\nu = \delta_c/\sigma$ ,  $\sigma^2$  is the smoothed variance of the matter power-spectrum,  $P(k)$ , given by

$$\sigma^2(R, z) = \frac{1}{2\pi^2} \int dk k^2 W^2(kR) P(k, z), \quad (3.2)$$

$W(kR)$  is the Fourier transform of the top-hat window function and  $R = \left(\frac{3M}{4\pi\rho_m}\right)^{1/3}$ .

The base form of the HMF fitted by the Euclid collaboration was proposed in [4] and is given by

$$\nu f(\nu)_E = A(p, q) \sqrt{\frac{2a\nu^2}{\pi}} \left(1 + \frac{1}{(a\nu^2)^p}\right) (\sqrt{a\nu})^{q-1} \exp\left(-\frac{a\nu^2}{2}\right). \quad (3.3)$$

The Euclid analysis has assumed that the parameters  $A$ ,  $p$ ,  $q$  and  $a$  have the following forms:

$$A(p, q) = \left\{ \frac{2^{-1/2-p+q/2}}{\sqrt{\pi}} \left[ 2^p \Gamma\left(\frac{q}{2}\right) + \Gamma\left(-p + \frac{q}{2}\right) \right] \right\}^{-1}, \quad (3.4)$$

$$a = a_R \Omega_m^{a_z} = \left[ a_1 + a_2 \left( \frac{d \ln \sigma}{d \ln R} + 0.6125 \right)^2 \right] \Omega_m^{a_z}, \quad (3.5)$$

$$p = p_1 + p_2 \left( \frac{d \ln \sigma}{d \ln R} + 0.5 \right), \quad (3.6)$$

$$q = \left[ q_1 + q_2 \left( \frac{d \ln \sigma}{d \ln R} + 0.5 \right) \right] \Omega_m^{q_z}, \quad (3.7)$$

where  $a_1$ ,  $a_2$ ,  $a_z$ ,  $p_1$ ,  $p_2$ ,  $q_1$ ,  $q_2$  and  $q_z$  are constants fitted with several N-body simulations discussed in [8]. The function  $A(p, q)$  normalises the HMF when  $p$  and  $q$  are constants.

As can be seen, the function  $a$  always multiplies  $\delta_c^2$  and depends both on redshift and mass scale. The usual SC model is scale-independent, therefore it is not able to explain the variation with mass scale, which is encoded in  $a_R$ . Thus, we will focus on the redshift dependence of the effective threshold,  $\Omega_m^{a_z} \delta_c^2$ , and analyse its relation with  $\delta_v$ .

The evolution of  $a\delta_c^2$  is shown in figure 1, where we used  $a_R = 0.7965$ , corresponding to a mass of  $10^{14} M_\odot h^{-1}$ . We can see that both  $\delta_v^2$  and  $a\delta_c^2$  increase at low- $z$ , so they qualitatively represent the same trend for halo formation, i.e., a threshold that increases as  $\Lambda$  becomes more important. Thus it is clear that the term  $\Omega_m^{a_z}$  inside  $a$  compensates the slight decay of  $\delta_c$  to better describe the abundance of simulated halos. Moreover,  $\delta_v^2$  is closer to  $a\delta_c^2$  than  $\delta_c^2$ . Therefore, also from a direct analysis of the E-HMF, one can conclude that the physics associated with the definition of  $\delta_v$  is more suitable than  $\delta_c$  because it gives a value closer to the effective threshold and grows at low- $z$ .

However, it is also clear that there exists a mismatch between  $\Omega_m^{a_z} \delta_c^2$  and  $\delta_v^2$ . We can see that the former grows faster at late times and  $a\delta_c^2$  has a lower value in the EdS limit. Our goal now is to find a representation of  $\Omega_m^{a_z} \delta_c^2$  in terms of  $\delta_v$  and later check whether it is robust against variations of  $\Omega_m^0$ . We could compare  $\Omega_m^{a_z} \delta_c^2$  and  $\delta_v^2$  directly, but as we will see this reparametrization will bring an important insight about the virialization model. Let us analyse the following description of the redshift-dependent part of the effective threshold

$$\Omega_m^{a_z} \delta_c^2(z) = \alpha \delta_v^\beta(z), \quad (3.8)$$

where  $\alpha$  and  $\beta$  are constants. It is important to note that this form will introduce a non-standard power-law dependence on the density threshold, i.e., distinct from power 2. This is unusual in the context of statistical derivation of HMF [1, 13], because the squared filtered density contrast has different power than its variance. One possible interpretation is that the extra powers of  $\delta_v$  encode the non-universality of HMF introduced by the new fitting

functions. This distinct power can also be understood as a hint that the actual dependence of the threshold on the virialization process has stronger time-dependence than predicted by the SC model. As we will show,  $\beta \simeq 4.37$  gives a representation of  $\Omega_m^{a_z} \delta_c^2$  that is precise and robust against variations of  $\Omega_m^0$ . We checked that when keeping the power 2 in the density threshold, the representation  $\Omega_m^{a_z} \delta_c^2(z) = \alpha \Omega_m^\beta \delta_v^2(z)$  gives better precision for a fixed  $\Omega_m^0$ , but is much less robust when varying  $\Omega_m^0$ .

The constant  $\alpha$  can be set by assuming that  $\Omega_m^{a_z} \delta_c^2 = \alpha \delta_v^\beta$  in the EdS limit, thus

$$\alpha = \frac{\delta_{c\text{EdS}}^2}{(\delta_{v\text{EdS}})^\beta}, \quad (3.9)$$

Then  $\beta$  is given by

$$\beta = \ln \left( \frac{\Omega_m^{a_z} \delta_c^2(z)}{\delta_{c\text{EdS}}^2} \right) / \ln \left( \frac{\delta_v(z)}{\delta_{v\text{EdS}}} \right). \quad (3.10)$$

which varies with  $z$ . For  $\Omega_m^0 = 0.3$  and  $0 \leq z \leq 2$ , we have  $4.05 < \beta < 4.51$ .

One could not expect that these two representations would match exactly. Nevertheless, we can compute an effective  $\beta$  that minimises the difference between them for some redshift interval of interest. We choose to minimise

$$\chi^2(\beta) = \sum_z \left[ \Omega_m^{a_z} \delta_c^2(z) - \delta_{c\text{EdS}}^2 \left( \frac{\delta_v(z)}{\delta_{v\text{EdS}}} \right)^\beta \right]^2. \quad (3.11)$$

taking the sum in redshift from  $z = 0$  to  $z = 2$  with 10 steps. We verified that concentrating the  $z$  interval at lower  $z$  does not change the results significantly. For  $\Omega_m^0 = 0.3$ , we get

$$\alpha = 0.3816 \text{ and } \beta = 4.3745. \quad (3.12)$$

Now let us see the level of agreement between the two representations. For convenience, we define:

$$D_c^2(z) \equiv \Omega_m^{a_z} \delta_c^2(z) \quad \text{and} \quad D_v^2(z) \equiv \alpha \delta_v^\beta(z). \quad (3.13)$$

In figure 2, we show the percent differences between  $D_v^2$  and  $D_c^2$  for several values of  $\Omega_m^0$ . We observe that the difference increases for lower  $\Omega_m^0$  values. This is expected because, when determining the parameter  $\alpha$ , we assumed EdS-limit, which is not well satisfied for low  $\Omega_m^0$ . On the other hand, the difference decreases for higher values of  $\Omega_m^0$ .

As can be seen, the representation of the redshift-dependent part of the effective threshold in the E-HMF is well described by a power-law function of  $\delta_v$ , even for values of  $\Omega_m^0$  distinct from the value used to determine the values of  $\alpha$  and  $\beta$ . This indicates that, within  $\Lambda$ CDM, the virialization threshold can consistently capture the redshift-dependence described in the E-HMF. From the fact that  $\Omega_m^{a_z} \delta_c^2(z) \propto \delta_v^{4.37}$ , we can expect that a more realistic SC model should provide a virialization threshold that grows faster at low- $z$ , but this analysis is beyond the scope of this paper.

#### 4 Sheth-Tormen halo mass function with $\delta_v$

Given that the redshift-dependent part of the effective threshold in the E-HMF is qualitatively similar to  $\delta_v$ , we might ask whether the use of the virialization threshold provides a better agreement between semi-analytic HMFs and the E-HMF, which currently is the most accurate

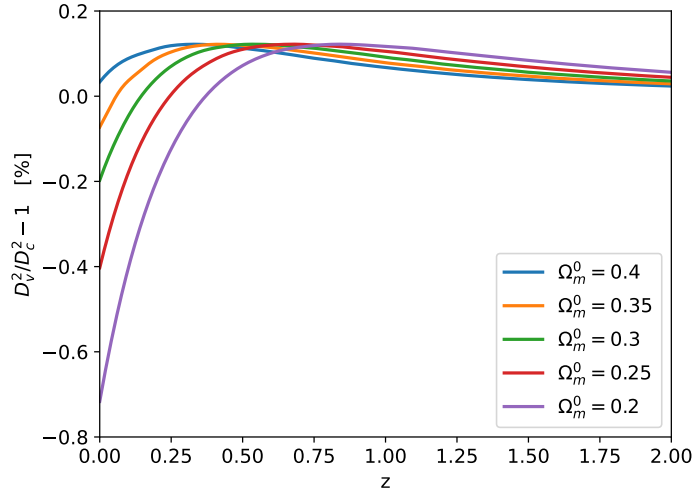


**Figure 2.** Difference between  $D_v^2$  and  $D_c^2$  defined in (3.13) for several values of  $\Omega_m^0$  indicated in the legend for  $\Lambda$ CDM model.

description of halo abundance for the  $\Lambda$ CDM model. Let us consider the ST-HMF [2], which has the form

$$\nu f(\nu)_{ST} = A \sqrt{\frac{2a\nu^2}{\pi}} \left( 1 + \frac{1}{(a\nu^2)^p} \right) \exp\left(-\frac{a\nu^2}{2}\right), \quad (4.1)$$

where  $a$  and  $p$  are constant fitted parameters,  $A(p) = [1 + 2^{-p}\Gamma(1/2 - p)/\sqrt{\pi}]^{-1}$  when assuming that the ST-HMF is normalised, or can be fitted as well.

The original values of the parameters are  $a = 0.707$ ,  $p = 0.3$  and  $A = 0.322$ . Besides many other refits of this HMF, more recently [6] produced a fit using the virialization overdensity given by [34], showing that identifying halos with this overdensity function provides a more universal HMF. The result for a fit considering all redshifts and models considered in that work is:

$$a = 0.7989, \quad p = 0.2536, \quad A = 0.3295. \quad (4.2)$$

The comparison made in [8] between their HMF and this fit indicates that, at  $z = 0$ , the two functions disagree by less than 5% up to roughly  $4.8 \times 10^{14} M_\odot h^{-1}$  and by less than 10% up to  $7 \times 10^{14} M_\odot h^{-1}$ . The differences increase at  $z = 1$  and  $z = 2$ .

Now let us refit these parameters with the substitution of  $\delta_c$  by  $\delta_v$ . First, we mention that a simple way to substitute  $\delta_c$  by  $\delta_v$  was given [26], where the original parameter  $a = 0.707$  was rescaled such that the EdS limit is the same, so

$$a \rightarrow \tilde{a} = a \frac{\delta_c^2 \text{EdS}}{\delta_v^2 \text{EdS}} \simeq 0.803, \quad (4.3)$$

maintaining  $p = 0.3$  and  $A(p) = [1 + 2^{-p}\Gamma(1/2 - p)/\sqrt{\pi}]^{-1}$  as a normalisation factor. We have verified that the reparametrization given by (4.3) deviates much more from the E-HMF than the one given by [6], equation (4.2). This deviation is mainly due to the high value of  $p$  used. As we will see, the preferred values of  $p$  with the virialization threshold is close to zero.



Assuming the E-HMF as fiducial HMF representation, we determine the new set of parameters by minimising

$$\chi^2(a, p, A) = \sum_{M, z} \left( \nu f(\nu)_{|STv} - \nu f(\nu)_{|E} \right)^2, \quad (4.4)$$

where  $\nu f(\nu)_{|E}$  is given by (3.3) and STv denotes (4.1) with the substitution  $\delta_c \rightarrow \delta_v$ . We take the mass summation between  $10^{14} M_\odot h^{-1}$  and  $10^{15} M_\odot h^{-1}$  with 10 log-spaced steps and the redshift summation with  $0 \leq z \leq 2$  in 10 steps. Note that this simple definition gives more weight to the differences at the peak of HMF at each redshift. The minimisation of (4.4) indicates

$$a = 0.8978, \quad p = 0.0031, \quad A = 0.3184. \quad (4.5)$$

We have verified that modifying the mass range in (4.4) to  $10^{13} - 10^{15} M_\odot h^{-1}$  with 10 log-spaced steps has small impact on the best-fit parameters, with a slight worsening of the fit. The range used for the determination of (4.5) was chosen for better accuracy at the high-mass tail, which is very sensitive to the cosmological model.

It is interesting to note that the PS limit of the ST-HMF is given by

$$a \rightarrow 1, \quad p \rightarrow 0, \quad A \rightarrow 1/2. \quad (4.6)$$

Therefore, as can be seen from the values in (4.5), refitting the ST-HMF with  $\delta_v$  produce parameters  $a$  and  $p$  that are much closer to the PS values than the original values or the more recent fit (4.2), while the parameter  $A$  has a very small change. Moreover, even when fitting for larger mass intervals, the parameters  $a$  and  $p$  still reach values closer to the PS limit when compared to the values of (4.2). This a concrete example that the use of  $\delta_v$  can provide HMF less dependent of external parameters.

In figure 3, we show the percent differences of ST and STv-HMFs against the E-HMF. The general trend is clear: the STv-HMF has better agreement with E-HMF than ST-HMF, except for some small intermediate mass interval. In particular, at  $z = 0$  and for  $\Omega_m^0 = 0.3$ , the deviation of STv from E-HMF is smaller than 1% for  $M < 1.8 \times 10^{14} M_\odot h^{-1}$  and for  $M > 4.4 \times 10^{14} M_\odot h^{-1}$  it is always smaller than ST-HMF.

Besides the improved agreement with the E-HMF, it is also important to note that, as expressed in [6], the residuals between their model and their numerical HMF “are larger at high  $\nu$ , where the best fit predicts more halos than we find in the simulations at  $z = 0$ .” Since  $\delta_v$  increases at low- $z$ , whereas  $\delta_c$  decreases, it is clear that a HMF with the virialization threshold is more suitable. This is also represented by the better agreement between STv and E-HMFs at higher masses, which occurs for all redshifts and values of  $\Omega_m^0$  shown in figure 3.

## 5 Beyond $\Lambda$ CDM models

As a further consistency check of the use of  $\delta_v$  as the threshold for halo formation in the ST template, we will analyse the level of agreement between E, ST and STv-HMFs when computing the impact of smooth DE models with  $w \neq -1$ . HMFs for smooth DE with varying equation of state parameter have been studied by [7], where the effects were modelled by an explicit dependence on the matter growth rate,  $f = d \ln \delta_m / d \ln a$ . However, as shown in [8], this HMF has an overall worse agreement with the E-HMF than the ST-HMF. It is also discussed that the dependence on  $f$  can be reparameterised in terms of  $\Omega_m$ , which appears

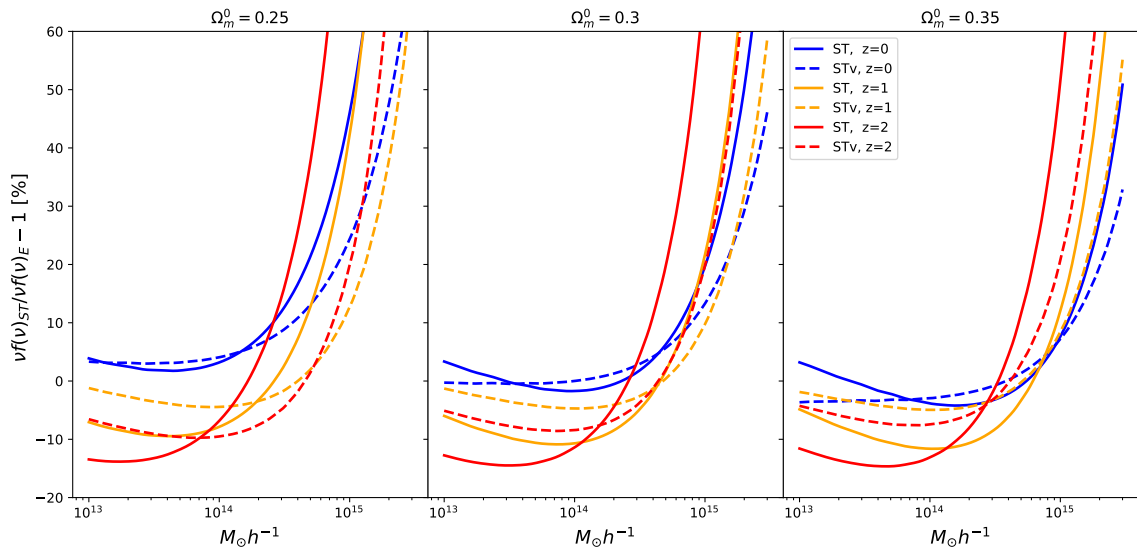


**Figure 3.** Differences between ST-HMF with parameters fitted using  $\delta_c$  (ST, solid lines), equation (4.2), and with  $\delta_v$  (STv, dashed lines), equation (4.5), with respect to the E-HMF, equation (3.3). Each panel shows the differences for distinct values of  $\Omega_m^0$ , indicated in the title of each plot, and for three redshifts indicated in the legend of the right panel.

in equation (3.5), making use of growth index parametrization  $f = \Omega_m^\gamma$ . Therefore, although the E-HMF has been fitted for the  $\Lambda$ CDM model, one can expect that the impact of  $w \neq -1$  can be consistently captured, and it will be used here as a basis of comparison.

A common technique used to extrapolate the validity of a fiducial HMF, numerically calibrated with simulations for a specific cosmological model, is to compute the comoving number density of halos as

$$\frac{dn}{dM}|_{\text{mod}} = R_n \frac{dn}{dM}|_{\text{fid}}, \quad (5.1)$$

where

$$R_n = \frac{dn/dM|_{\text{mod}}}{dn/dM|_{\text{ref. mod}}}, \quad (5.2)$$

is computed with an HMF for which some analytical model can be used to describe the features of the cosmological model under consideration (indicated by the ‘mod’ subscript) and its counterpart for the reference model (‘ref. mod’ subscript,  $\Lambda$ CDM in our case), see, e.g., [26, 35–37].

In order to explore the impact of smooth DE models beyond  $\Lambda$ , we compute how a particular HMF for  $w \neq -1$  changes with respect to the one for the  $\Lambda$ CDM model. As explained earlier, the E-HMF should provide a good representation for them. In this case, one would not need to compute  $R_n$ , and the E-HMF could be used directly with the quantities associated with the new model. In what follows, we also compute  $R_n$  for the E-HMF as a reference for comparison with the results for ST and STv-HMFs. In the following examples, we assume the  $w_0 w_a$  parametrization for the equation of state parameter (EoS) [38, 39]

$$w(a) = w_0 + w_a(1 - a). \quad (5.3)$$

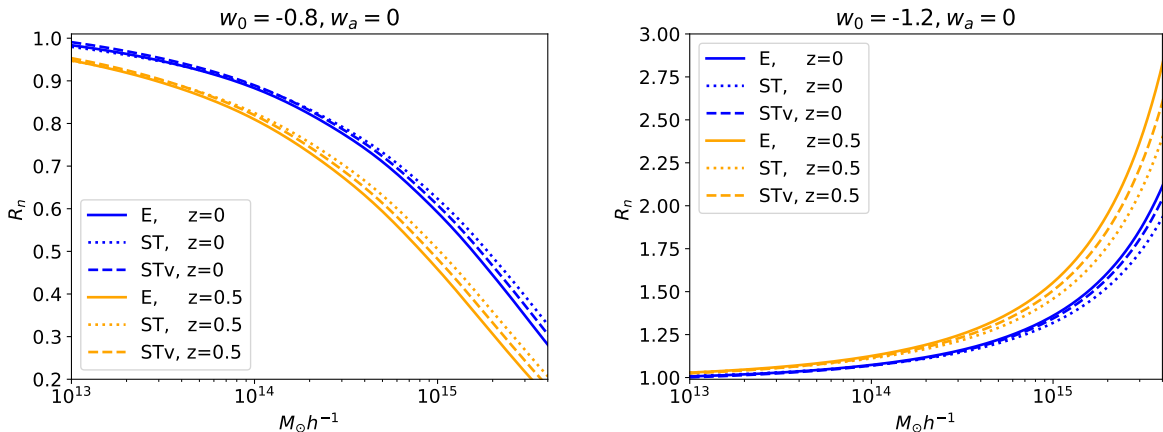


**Figure 4.**  $R_n$ , defined in (5.2), for STv, ST and E-HMFs (indicated in the plot legends) for dark energy models with  $w_0 = -0.8$  (left panel) and  $w_0 = -1.2$  (right panel) at  $z = 0$  (blue lines) and  $z = 0.5$  (orange lines). (5.2)

### 5.1 Constant EoS

In figure 4 we show  $R_n$  for ST, STv and E-HMF for  $w_0 = -0.8$  and  $w_0 = -1.2$ , with  $w_a = 0$  in both cases. As can be seen, all the HMFs agree qualitatively, showing a decrease of the comoving number density of halos for  $w_0 = -0.8$  and a increase for  $w_0 = -1.2$ . We also note that STv-HMF has an overall better agreement with E-HMF than ST-HMF, especially for high masses. Therefore, we can conclude that the use of  $\delta_v$  in ST template also provides better agreement with E-HMF for smooth DE models with  $w_0 \neq -1$  and  $w_a = 0$ . Moreover, it is also evident that the impact of  $w_0$  in ST-HMF is the smallest at high masses. This happens because ST-HMF effective threshold is essentially constant, so the impact of distinct DE models is captured only by the linear evolution of perturbations, encoded in  $\sigma(M, z)$ .

An important feature to note in these examples is the clear impact of phantom ( $w < -1$ ) and non-phantom EoS ( $w > -1$ ) with respect to  $\Lambda$ CDM. For  $w_0 = -0.8$ , the DE fluid has more energy density than  $\Lambda$  at high- $z$ , consequently  $\Omega_m(z)$  is lower and the growth of matter fluctuations is relatively suppressed. As a consequence, we always have  $R_n < 1$ . The opposite occurs for the phantom case of  $w_0 = -1.2$ .

### 5.2 Time varying EoS

Although the impact of constant EoS is very clear, and all the three HMFs agree qualitatively about it, the situation for time-varying EoS can be more complex. As an example, we will analyse two pairs of  $(w_0, w_a)$  values, whose growth history changes in time with respect to the  $\Lambda$ CDM one. For  $p_1 = (w_0 = -0.9, w_a = -0.3)$  the EoS is phantom at high- $z$  and non-phantom at low- $z$ . For  $p_2 = (w_0 = -1.104, w_a = 0.3)$ , the converse holds. It is interesting to note that the first kind of EoS evolution is supported by the recent DESI-BAO analysis [40].

Let us first analyse the relative linear growth history with respect to  $\Lambda$ CDM. In figure 5, we show the ratio between the evolutions of  $\sigma_8(z)$ , given by

$$R_{\sigma_8} = \frac{\sigma_8(z)_{\text{mod}}}{\sigma_8(z)_{\Lambda\text{CDM}}}. \quad (5.4)$$

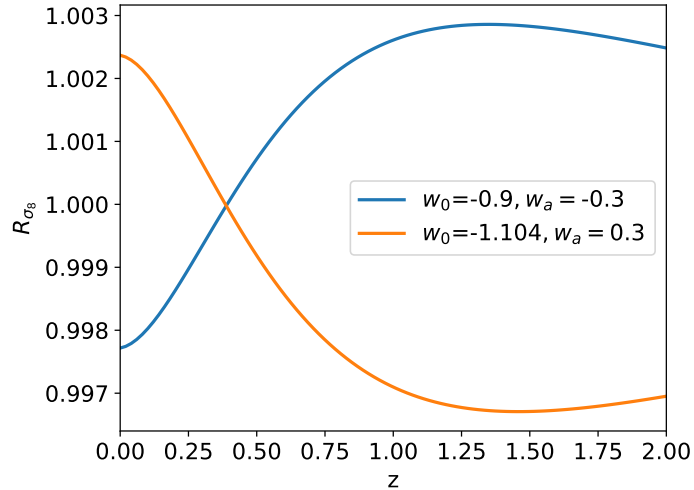


**Figure 5.** Evolution of  $R_{\sigma_8}(z)$ , defined in (5.4), for two pairs of  $w_0$  and  $w_a$  indicated in the plot legend.

For  $p_1$ ,  $\sigma_8$  is higher than in  $\Lambda$ CDM at high- $z$ . At lower  $z$ , the EoS becomes non-phantom and there is less growth with respect to  $\Lambda$ CDM. The opposite happens for  $p_2$ . In both cases, this relative transition in the growth behaviour occurs at  $z_t \simeq 0.38$  (the value of  $w_0$  in  $p_2$  was adjusted to get approximately the same  $z_t$  as for  $p_1$ ).

Prior to  $z_t \simeq 0.38$ , the growth histories of the two examples are clearly enhanced or diminished with respect to  $\Lambda$ CDM. It is not expected that the nonlinear evolution encoded in the effective threshold of HMFs should present a distinct relative behaviour as seen for  $R_{\sigma_8}$ . Therefore, at  $z > z_t$ , the ratio between halo number densities, equation (5.2), should preserve the relations seen in figure 5.

However, these relations between models based on the linear growth history is not always satisfied by HMFs. In figure 6 we show  $R_n$  for the two models considered in this subsection. As can be seen, at  $z = 0.4$ , slightly before  $z_t \simeq 0.38$ , only ST-HMF presents the expected behaviour:  $R_n > 1$  for  $p_1$  and  $R_n < 1$  for  $p_2$ . This is easy to understand, given that the effective threshold in the ST-HMF depends on  $\delta_c$ , which is nearly constant, the main impact in  $R_n$  is due to  $\sigma(M, z)$ . For STv and E-HMF, the effective thresholds vary in time, but in a manner not totally consistent with the variation of  $\sigma_8(z)$ .

As can be seen in figure 6, at  $z = 0$ , all three HMFs agree qualitatively. We have also verified that, for both  $p_1$  and  $p_2$ , STv-HMF has the expected  $R_n$  for  $z > 0.46$  and E-HMF for  $z > 0.51$ . For  $z > 0.51$ , all three HMFs agree about the impact of EoS in number density with respect to  $\Lambda$ CDM. We also have checked the behaviour of  $R_n$  given by the HMF proposed in [7], finding very similar results to the ones observed for ST-HMF. This is expected because the HMF proposed in [7] considers multiplicative corrections on the ST template.

In order to clearly see that this undesirable effect is caused by the effective threshold, in figure 7, we show the redshift evolution of the ratios

$$R_c = \frac{D_{c \text{ mod}}}{D_{c \Lambda}} \quad \text{and} \quad R_v = \frac{\delta_{v \text{ mod}}}{\delta_{v \Lambda}}, \quad (5.5)$$

where  $D_c$  is the time-dependent part of the effective threshold in the E-HMF, defined in

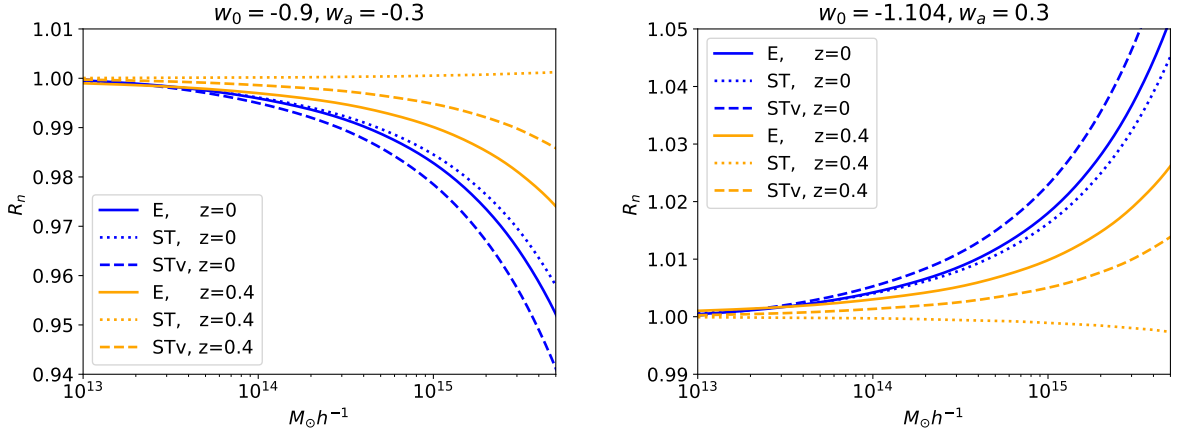


**Figure 6.** Ratios of STv, ST and E-HMFs (indicated in the plot legends) for DE models with EoS parameters indicated at the plot titles at  $z = 0$  (blue lines) and  $z = 1$  (orange lines).

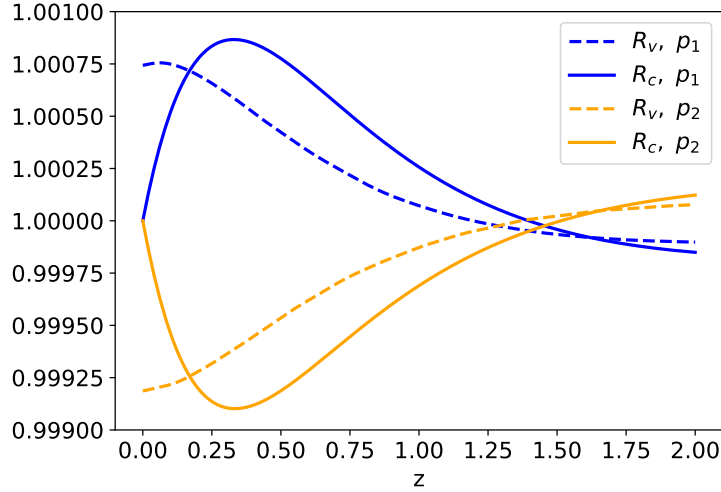


**Figure 7.** Evolution of  $R_c - 1$  and  $R_v - 1$ , defined in (5.5), for  $p_1 = (w_0 = -0.9, w_a = -0.3)$  and  $p_2 = (w_0 = -1.104, w_a = 0.3)$ .

(3.13). At high- $z$ , both quantities are lower than unity for  $p_1$  and higher than unity for  $p_2$ , as expected for enhanced and diminished growth histories with respect to  $\Lambda$ CDM, respectively. The inversion in the relative behaviour occurs much earlier than the one related to  $\sigma_8(z)$ , shown in figure 5. After this inversion,  $R_v$  remains above or lower the unity, whereas  $R_c \rightarrow 1$  as  $z \rightarrow 0$ . Moreover,  $R_c$  reaches higher or lower values than  $R_v$ , with a stronger time variation.

Although these differences with respect to  $\Lambda$ CDM are small, when compared to  $R_{\sigma_8}$  variations, the behaviour of  $R_c$  and  $R_v$  do not totally agree with  $R_{\sigma_8}$  shown in figure 5. Inversions in  $R_c$  and  $R_v$  occur much earlier than the ones for  $R_{\sigma_8}$ . This would indicate that the relative inversion in the effective threshold, which encodes the nonlinear evolution, can anticipate the one associated with the linear evolution, encoded in  $\sigma_8(z)$ , which looks highly unlikely to be true.

Moreover,  $R_c$  shows a second problem. Given that the redshift evolution of the effective threshold in the E-HMF mainly depends on  $\Omega_m^{a_z}$ , for fixed  $\Omega_m^0$ ,  $R_c$  for different models have the same value at  $z = 0$ . This looks unnatural and is in disagreement with behaviour  $R_{\sigma_8}$  shown in figure 5. Such behaviour would indicate that, although a specific model has more/less linear growth than  $\Lambda$ CDM at low- $z$ , the effective threshold does not respond to this increase/decrease of growth at low- $z$ . This issue might indicate that the parameter  $a_z$  in the E-HMF should have some dependence on the EoS. On the other hand,  $R_v$  reproduces the behaviour of  $R_{\sigma_8}$  at low- $z$ , what looks more natural.

However, it is important to note that these theoretical issues with the models with time-varying EoS might not be problematic when confronted with observational or simulated data. For the two cases analysed, the undesirable behaviour of  $R_n$  occurs at intermediate redshifts ( $0.4 \lesssim z \lesssim 0.5$ ) with more impact for the most massive halos, which are not so abundant early on. In general, and as expected, the differences in  $R_n$  between HMFs increase at high masses, but exceed 1% only for rare objects, e.g.,  $M > 2 \times 10^{15} M_\odot h^{-1}$  at  $z = 0$  or  $M > 1 \times 10^{15} M_\odot h^{-1}$  at  $z = 0.4$ . Moreover, the actual number of observed clusters also depend on the comoving volume, which is analytically determined and can have large variations with the EoS.

## 6 Conclusions

We have analysed the redshift dependence of the effective threshold in the E-HMF, proposed in [8], showing it is qualitatively equivalent to the virialization threshold,  $\delta_v$ , and incompatible with the evolution of the collapse threshold,  $\delta_c$ , which has been used in many HMFs so far. This finding indicates that the abundance of halos in the Universe is better described by the physics of virialization, encoded in  $\delta_v$ , than physics of collapse, associated with  $\delta_c$ .

We found that the redshift-dependent part of the E-HMF,  $\Omega_m^{a_z} \delta_c^2$ , can be accurately represented by a simple power-law function of the virialization threshold, given by  $\alpha \delta_v^\beta$ , which is also robust against variations of  $\Omega_m^0$ , showing that the natural dependence of the threshold on  $\delta_v$  is not a coincidence for a particular expansion history in the  $\Lambda$ CDM model. We found  $\beta \simeq 4.37$ , which shows that the effective threshold in the E-HMF grows faster than  $\delta_v^2$  at low- $z$ . We interpret this as an indication that a more realistic model for the nonlinear dynamics and virialization should provide faster growing  $\delta_v$ , in such a way that effective threshold is proportional to the square of this new function, as demanded by the analytical formulation of the HMF.

Exploring these findings, we have shown that a refitted ST-HMF with the substitution  $\delta_c \rightarrow \delta_v$  has better agreement with the E-HMF, which is also robust when varying  $\Omega_m^0$ . Interestingly, this refit increases the parameter  $a$  and decreases the parameter  $p$ , showing that the deviation of the ST-HMF with  $\delta_v$  from the PS-HMF is smaller. This is a concrete example that the use of the virialization threshold in HMFs is more natural and can diminish their dependence on extra parameters.

We also analysed the case of smooth DE with constant and time-varying EoS. For constant  $w$ , all the three HMF under consideration (ST, STv and E-HMF) agree qualitatively about the relative abundance number density of halos with respect to  $\Lambda$ CDM. In this case, the changes in  $\sigma(M, z)$  are more relevant than the ones in the effective threshold. In this scenario, the STv-HMF has a better agreement with E-HMF than ST-HMF for both phantom and non-phantom EoS in the mass range under consideration.

The case of time-varying EoS is more complex. Considering two examples of the  $w_0 w_a$  parametrization that transit from phantom to non-phantom regimes, and vice-versa, we

showed that the impact of time-varying EoS in the STv and E-HMFs is not totally consistent with the linear growth history encoded in  $\sigma_8(z)$ . Moreover, in these examples, the time-dependent part of the effective threshold in E-HMF approaches the same value as in  $\Lambda$ CDM at  $z = 0$ , in qualitative disagreement with the behaviour of  $\sigma_8(z)$  for distinct models. However, given the small deviations from the expected behaviour and that their impact occurs mostly at the high-mass tail of the HMFs, it is likely that the observational consequences of this issue are very small, or even negligible.

Our main conclusion is that the virialization threshold is a sensible basic model for the description of the time-dependence of the effective threshold for smooth DE models. Given that  $\delta_v$  is computed by a physical model, in principle, it should provide a reliable manner to determine the impact models beyond smooth DE in halo abundances, such as clustering DE, or even for the scenarios of modified gravity and models beyond cold dark matter. Furthermore, at least in the case of clustering DE, it is not numerically possible to compute  $\delta_c$  [29], thus the use of  $\delta_v$  is essential to explore the behaviour of such models with semi-analytic HMFs.

## Acknowledgments

RCB thanks Valerio Marra for useful discussions and Tiago Castro for critical analysis of several ideas in this work.

## A $\delta_v$ fit for $\Lambda$ CDM and a general code for its computation

It might be helpful to determinate a representation of  $\delta_v$  in terms of  $\delta_c$  for the  $\Lambda$ CDM model, because the latter has a simple and well-known fitting function, given by [21]. We proceed with the following representation

$$\delta_v = \alpha \delta_c^\beta \quad (\text{A.1})$$

and determine the constant values  $\alpha$  and  $\beta$ . We assume that  $\delta_v$  and  $\alpha \delta_c^\beta$  match in the EdS limit, so we have the analogous of equation (3.9) for  $\alpha$  and

$$\beta = \frac{\ln(\delta_v/\delta_{v\text{EdS}})}{\ln(\delta_c/\delta_{c\text{EdS}})}. \quad (\text{A.2})$$

For  $\Omega_m^0 = 0.3$  and  $0 < z < 2$ , we have  $-2.27 > \beta > -2.55$ . We compute an effective value in the same way as in equation (3.11), getting

$$\alpha = 5.4078 \quad \text{and} \quad \beta = -2.3509. \quad (\text{A.3})$$

In figure 8, we show the percent difference between the numerical solution and the fit given by (A.1). As can be seen, this representation of  $\delta_v$  is very precise and robust when varying  $\Omega_m^0$ , with error below 0.17% for  $0.2 \leq \Omega_m^0 < 0.4$ .

Moreover, a code to compute the evolution of matter fluctuations in the SC model and the determination of the virialization threshold,  $\delta_v$ , for smooth DE models described by the  $w_0 w_a$  parametrization is publicly available at <https://github.com/roncab/scollas>.

## References

- [1] W. H. Press and P. Schechter, *Formation of galaxies and clusters of galaxies by selfsimilar gravitational condensation*, *Astrophys. J.* **187** (1974) 425–438.



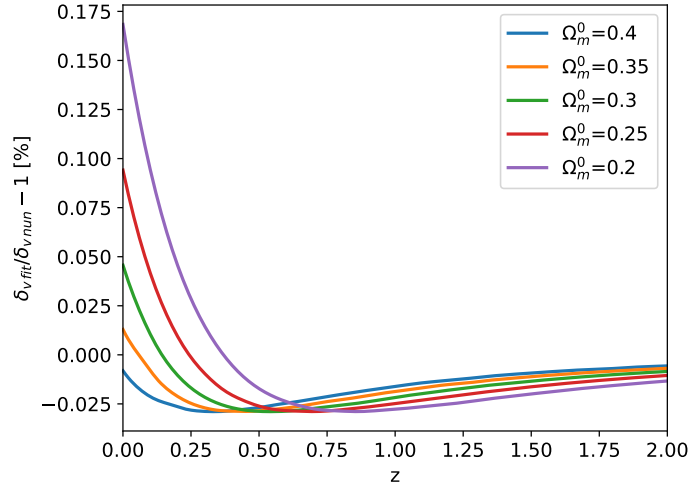


**Figure 8.** Percent difference between the representation of  $\delta_v$  given by (A.1) and its numerical solution in the  $\Lambda$ CDM model for several values of  $\Omega_m^0$  indicated in the plot legend.

- [2] R. K. Sheth and G. Tormen, *Large-scale bias and the peak background split*, *MNRAS* **308** (Sept., 1999) 119–126, [[astro-ph/](#)].
- [3] J. L. Tinker, A. V. Kravtsov, A. Klypin, K. Abazajian, M. S. Warren, G. Yepes, S. Gottlober, and D. E. Holz, *Toward a halo mass function for precision cosmology: The Limits of universality*, *Astrophys. J.* **688** (2008) 709–728, [[arXiv:0803.2706](#)].
- [4] S. Bhattacharya, K. Heitmann, M. White, Z. Lukic, C. Wagner, and S. Habib, *Mass function predictions beyond lcdm*, *Astrophys. J.* **732** (2011) 122, [[arXiv:1005.2239](#)].
- [5] W. A. Watson, I. T. Iliev, A. D’Aloisio, A. Knebe, P. R. Shapiro, and G. Yepes, *The halo mass function through the cosmic ages*, *Mon. Not. Roy. Astron. Soc.* **433** (2013) 1230, [[arXiv:1212.0095](#)].
- [6] G. Despali, C. Giocoli, R. E. Angulo, G. Tormen, R. K. Sheth, G. Baso, and L. Moscardini, *The universality of the virial halo mass function and models for non-universality of other halo definitions*, *Mon. Not. Roy. Astron. Soc.* **456** (2016), no. 3 2486–2504, [[arXiv:1507.0562](#)].
- [7] L. Ondaro-Mallea, R. E. Angulo, M. Zennaro, S. Contreras, and G. Aricò, *Non-universality of the mass function: dependence on the growth rate and power spectrum shape*, *Mon. Not. Roy. Astron. Soc.* **509** (2021), no. 4 6077–6090, [[arXiv:2102.0895](#)].
- [8] **Euclid** Collaboration, T. Castro *et. al.*, *Euclid preparation. XXIV. Calibration of the halo mass function in  $\Lambda(\nu)$ CDM cosmologies*, *Astron. Astrophys.* **671** (2023) A100, [[arXiv:2208.0217](#)].
- [9] M. Asgari, A. J. Mead, and C. Heymans, *The halo model for cosmology: a pedagogical review*, [[arXiv:2303.0875](#)].
- [10] G. Efstathiou, S. M. Fall, and C. Hogan, *Self-similar gravitational clustering*, *Monthly Notices of the Royal Astronomical Society* **189** (11, 1979) 203–220, [<https://academic.oup.com/mnras/article-pdf/189/2/203/2830905/mnras189-0203.pdf>].
- [11] S. Colafrancesco, F. Lucchin, and S. Matarrese, *The mass function from local density maxima. groups and clusters of galaxies*, *Astrophys. J.* **345** (1989) 3–11.
- [12] J. M. Gelb and E. Bertschinger, *Cold dark matter. 1: The formation of dark halos*, *Astrophys. J.* **436** (1994) 467, [[astro-ph/9408028](#)].



- [13] J. M. Bardeen, J. R. Bond, N. Kaiser, and A. S. Szalay, *The statistics of peaks of gaussian random fields*, *Astrophys. J.* **304** (1986) 15–61.
- [14] J. R. Bond, S. Cole, G. Efstathiou, and N. Kaiser, *Excursion set mass functions for hierarchical gaussian fluctuations*, *Astrophys. J.* **379** (1991) 440.
- [15] J. E. Gunn and J. R. I. Gott, *On the infall of matter into cluster of galaxies and some effects on their evolution*, *Astrophys. J.* **176** (1972) 1–19.
- [16] T. Padmanabhan, *Structure Formation in the Universe*. Cambridge University Press, 1993.
- [17] R. K. Sheth, H. J. Mo, and G. Tormen, *Ellipsoidal collapse and an improved model for the number and spatial distribution of dark matter haloes*, *Mon. Not. Roy. Astron. Soc.* **323** (2001) 1, [[astro-ph/9907024](#)].
- [18] T. Castro, V. Marra, and M. Quartin, *Constraining the halo mass function with observations*, *Mon. Not. Roy. Astron. Soc.* **463** (2016), no. 2 1666–1677, [[arXiv:1605.0754](#)].
- [19] P. B. Lilje, *Abundance of Rich Clusters of Galaxies: A Test for Cosmological Parameters*, *Astrophysical Journal Letters* **386** (Feb., 1992) L33.
- [20] C. Lacey and S. Cole, *Merger rates in hierarchical models of galaxy formation*, *Mon. Not. Roy. Astron. Soc.* **262** (June, 1993) 627–649.
- [21] T. Kitayama and Y. Suto, *Semianalytical predictions for statistical properties of x-ray clusters of galaxies in cold dark matter universes*, *Astrophys. J.* **469** (1996) 480, [[astro-ph/9604141](#)].
- [22] A. Mead, J. Peacock, C. Heymans, S. Joudaki, and A. Heavens, *An accurate halo model for fitting non-linear cosmological power spectra and baryonic feedback models*, *Mon. Not. Roy. Astron. Soc.* **454** (2015), no. 2 1958–1975, [[arXiv:1505.0783](#)].
- [23] S. Lee, *Spherical collapse model with and without curvature*, *Physics Letters B* **685** (Mar, 2010) 110–114.
- [24] S. Lee and K.-W. Ng, *Spherical collapse model with non-clustering dark energy*, *JCAP* **1010** (2010) 028, [[arXiv:0910.0126](#)].
- [25] S. Lee and K.-W. Ng, *Cluster number counts in quintessence models*, [[arXiv:1010.2291](#)].
- [26] R. C. Batista and V. Marra, *Clustering dark energy and halo abundances*, *JCAP* **11** (2017) 048, [[arXiv:1709.0342](#)].
- [27] C.-C. Chang, W. Lee, and K.-W. Ng, *Spherical Collapse Models with Clustered Dark Energy*, *Phys. Dark Univ.* **19** (2018) 12–20, [[arXiv:1711.0043](#)].
- [28] R. C. Batista, *A Short Review on Clustering Dark Energy*, *Universe* **8** (2021), no. 1 22, [[arXiv:2204.1234](#)].
- [29] R. C. Batista, H. P. de Oliveira, and L. R. W. Abramo, *Spherical collapse of non-top-hat profiles in the presence of dark energy with arbitrary sound speed*, *JCAP* **02** (2023) 037, [[arXiv:2210.1476](#)].
- [30] A. Lewis, A. Challinor, and A. Lasenby, *Efficient computation of cmb anisotropies in closed frw models*, *Astrophys. J.* **538** (2000) 473–476, [[astro-ph/9911177](#)].
- [31] T. Basse, O. E. Bjaelde, S. Hannestad, and Y. Y. Y. Wong, *Confronting the sound speed of dark energy with future cluster surveys*, [[arXiv:1205.0548](#)].
- [32] D. F. Mota and C. van de Bruck, *On the spherical collapse model in dark energy cosmologies*, *Astron. Astrophys.* **421** (2004) 71–81, [[astro-ph/0401504](#)].
- [33] I. Maor and O. Lahav, *On virialization with dark energy*, *JCAP* **0507** (2005) 003, [[astro-ph/0505308](#)].
- [34] G. L. Bryan and M. L. Norman, *Statistical properties of x-ray clusters: Analytic and numerical comparisons*, *Astrophys. J.* **495** (1998) 80, [[astro-ph/9710107](#)].

- [35] M. LoVerde, A. Miller, S. Shandera, and L. Verde, *Effects of Scale-Dependent Non-Gaussianity on Cosmological Structures*, *JCAP* **0804** (2008) 014, [[arXiv:0711.4126](#)].
- [36] P. Creminelli, G. D’Amico, J. Norena, L. Senatore, and F. Vernizzi, *Spherical collapse in quintessence models with zero speed of sound*, *JCAP* **1003** (2010) 027, [[arXiv:0911.2701](#)].
- [37] R. Batista and F. Pace, *Structure formation in inhomogeneous Early Dark Energy models*, *JCAP* **1306** (2013) 044, [[arXiv:1303.0414](#)].
- [38] M. Chevallier and D. Polarski, *Accelerating universes with scaling dark matter*, *Int. J. Mod. Phys.* **D10** (2001) 213–224, [[gr-qc/0009008](#)].
- [39] E. V. Linder, *Exploring the expansion history of the universe*, *Phys. Rev. Lett.* **90** (2003) 091301, [[astro-ph/0208512](#)].
- [40] **DESI** Collaboration, A. G. Adame *et. al.*, *Desi 2024 vi: Cosmological constraints from the measurements of baryon acoustic oscillations*, [arXiv:2404.0300](#).